PCCP

Reconstitution of nanopores in bilayers of diblock and triblock copolymers

Journal:	*Physical Chemistry Chemical Physics*
Manuscript ID	CP-ART-12-2024-004782.R1
Article Type:	Paper
Date Submitted by the Author:	14-Apr-2025

Complete List of Authors:	Kihara, Hiroaki; Tokyo University of Agriculture and Technology, Department of Biotechnology and Life Science Sato, Mikiyoshi; Tokyo University and Agriculture and Technology, Department of Biotechnology and Life Science Kawano, Ryuji; Tokyo University and Agriculture and Technology, Department of Biotechnology and Life Science

Reconstitution of nanopores in bilayers of diblock and triblock copolymers

Hiroaki Kihara, Mikiyoshi Sato, and Ryuji Kawano*

Department of Biotechnology and Life Science, Tokyo University and Agriculture and Technology, Tokyo Japan

*Corresponding author: rjkawano@cc.tuat.ac.jp

Abstract.

This study investigates the properties of bilayer polymer membranes (BPMs) formed from four amphiphilic block copolymers, PBD11, PBD22, PDMS22, and PDMS35, and their interactions with nanopores. Using the droplet contact method in microdevices, we systematically evaluated key membrane characteristics, including stability, hydrophobic thickness, bilayer tension, and adhesive energy. The results revealed that PBD-series polymers exhibited superior stability under time and voltage stress compared to PDMS-series polymers. Importantly, correlation analysis identified a strong relationship between the adhesive energy ratio ($\Delta F/2\gamma_m$) and membrane stability (R^2=0.88), indicating $\Delta F/2\gamma_m$ as a promising predictive parameter for membrane properties. Additionally, the reconstitution of α-hemolysin (αHL) nanopores was achieved with PBD11 and PDMS35, underscoring the critical role of matching membrane hydrophobic thickness to nanopore dimensions. Notably, PBD11 demonstrated reduced electrical noise and was compatible with the artificial nanopore SVG28. These findings offer valuable insights into optimizing BPM properties for nanopore sensing, paving the way for future innovations in synthetic nanopore technology.

Introduction

Nanopore sensing has emerged as a promising approach for the electrical and label-free detection of molecules. In this technology, a pore-forming transmembrane protein is reconstituted in a planar lipid bilayer, and the target molecules can be detected at the single molecule level by recording the ion currents generated as they pass through the pore.[1–3] Nanopore technology has been applied to organic molecules, oligonucleotides, and protein detection and has recently been commercialized as the nanopore DNA sequencer.[2,4]

An intriguing feature of nanopore technology is that the pore-forming protein is not the sensing material in its natural state. Many of the nanopore proteins are pore-forming toxins,[5] and they form nanopore structures within cell membranes inducing cell lysis; they do not function as sensors in nature. In the 1990s, researchers found these proteins from nature and employed them as electrical sensors based on the Colter counter technique, utilizing them as an artificial device.[3] Instead of using natural pore proteins, recent advancements have focused on the development of synthetic nanopores, including those created through *de novo* design of proteins/DNAs, which have been reconstituted in phospholipid bilayer membranes.[6–9] With regard to the lipid membrane from an artificial perspective, DPhPC is an artificially modified lipid molecule that improves the stability of the planar lipid membrane. Synthetic polymers with amphiphilic properties that adopt a liquid crystalline phase have also been employed to prepare the planar bilayer membrane.[10–16] These amphiphilic polymers have been employed as the material for vesicles instead of lipid vesicles, resulting in the formation of artificial vesicles, or polymersomes. Concurrently, such polymers have been applied to planar polymer membranes. These polymers can be regarded as higher molecular weight analogs of lipids and may lead to the formation of unique membrane structures that are inaccessible to conventional lipids.

Two decades of preliminary research into polymer membranes has yielded encouraging results, [10–16] with recent studies successfully demonstrating the reconstitution of nanopores into polymer membranes.[11,12,16] In comparison to bilayer lipid membranes (BLMs), polymer membranes demonstrate enhanced mechanical and chemical stability, which makes them a viable candidate for the creation of artificial membranes for nanopore technology.[17] The characteristics of the polymers including the monomer

species, molecular weight, and the presence of di- or tri-block configuration, can be tuned to achieve the desired properties. The mechanical and thermal stability of these membranes improves the distribution and usability of the device.

Here, we investigate the membrane stability and other properties related to nanopore measurements in four synthetic polymers (**Fig. 1**) using the droplet contact method (DCM) in a microdevice.[18,19]

1) PBD_{11}-*b*-PEO_8 (PBD11)
2) PBD_{22}-*b*-PEO_{14} (PBD22)
3) $PDMS_{22}$-*b*-$PMOXA_6$ (PDMS22)
4) $PMOXA_{11}$-*b*-$PDMS_{35}$-*b*-$PMOXA_{11}$ (PDMS35)

PBD: poly(1,2-butadine)
PEO: poly(ethylene oxide)
PDMS: poly(dimethylsiloxane)
PMOXA: poly(2-methyloxazoline)
*Number (PBD_m-*b*-PEO_n): unit number

We selected four polymers from the following three aspects:

1) Polymer length (PBD11 and PBD22):

Despite having similar chemical structures, PBD11 and PBD22 differ in the length of their polymer chains.

2) Monomer types (PDMS22 and the PBD series):

Despite both having a di-block configuration, PDMS22 and the PBD series have disparate chemical structures,

3) Di- and tri-block configurations (PDMS22 and PDMS35):

Despite having a similar chemical structure to PDMS22, PDMS35 is a tri-block configuration.

Although it has been reported that both monolayer (I-type) and bilayer (U-type) structures coexist in the planar membranes of PMOXA-*b*-PDMS-*b*-PMOXA[20], four types of polymer membranes were referred to as bilayer polymer membranes (BPMs) in this

study. Our investigation yielded insights into the membrane properties of four BPMs, including bilayer tension, adhesive energy, membrane thickness, membrane lifetime, stability under voltage application, and the effect of polymer composition. Additionally, we explored the reconstitution of αHL nanopores in relation to pore-forming activity, electrical noise, and pore size. Finally, the pore formation activity of artificial nanopores into PBD11 was examined. This approach holds promise for streamlining the preparation of diverse BPMs and evaluating nanopores integrated within BPMs.

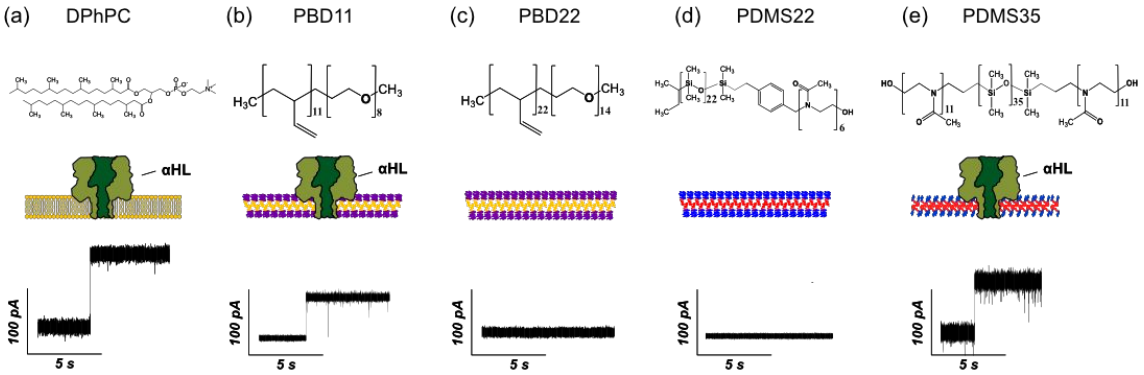

Fig. 1 (a-e) The molecular structure and the typical current-time trace of BLMs and BPMs.

Material method

Reagents and chemicals

In this study, we used the following reagents: 1,2-diphytanoyl-*sn*-glycero-3-phosphocholine (DPhPC; Avanti. Polar Lipids, Alabaster, AL, USA), chloroform (Nacalai Tesque.INC, Kyoto, JAPAN), *n*-decane (decane; Wako Pure Chemical Industries, Ltd., Osaka, Japan), potassium chloride (KCl; Nacalai Tesque, Kyoto, Japan), 3-morpholinopropane-1-sulfonic acid (MOPS; Nacalai Tesque, Kyoto, Japan), dimethyl sulfoxide (DMSO, FUJIFILM Wako Pure Chemical Industries, Ltd. (Wako), Japan), potassium hydroxide (KOH, FUJIFILM Wako Pure Chemical Industries, Ltd. (Wako), hydrochloric acid (HCl, FUJIFILM Wako Pure Chemical Industries, Ltd. (Wako) Japan). Four amphiphilic block copolymers were as follows: poly(2-methyloxazoline)-*b*-poly(dimethylsiloxane)-*b*-poly(2-methyloxazoline), abbreviated as PMOXA-*b*-PDMS-*b*-PMOXA (950 g/mol-*b*-2600 g/mol-*b*-950 g/mol, repeat unit: 11-*b*-35-*b*-11, Product ID:

P10918A-MOXZDMSMOXZ), poly(dimethylsiloxane)-*b*-poly(2-methyloxazoline), abbreviated as PDMS-*b*-PMOXA (1600 g/mol-*b*-500 g/mol, repeat unit: 22-*b*-6, Product ID: P43344C-DMSMEOXZ), poly(1,2-butadiene)-*b*-poly(ethylene oxide), PBD-*b*-PEO (1200 g/mol-*b*-600 g/mol, repeat unit: 22-*b*-14, Product ID: P41745- BdEO, 600 g/mol-*b*-350 g/mol, repeat unit: 11-*b*-8, Product ID: P41807C-BdEO). All block copolymers were obtained from Polymer Source Inc.

Buffered electrolyte solutions (1 M KCl, 10 mM MOPS at pH 7.0) were prepared using ultrapure water, which was obtained from a Milli-Q system (Millipore, Billerica, MA, USA). Two oil compositions are used in this study: decane and a 3:7 (v:v) mixture of decane and chloroform. DPhPC in chloroform was first evaporated, and decane was added to a final concentration of 10 mg/mL (DPhPC solution). The polymers were first completely dissolved in chloroform, and then decane was added in a chloroform: decane volume ratio of 3:7 (v:v), resulting in a final polymer concentration of 7.5 mg/mL. Wild-type alpha-hemolysin (αHL; Sigma Aldrich, St. Louis, MO, USA and List Biological Laboratories, Campbell, CA, USA) was obtained as the monomer polypeptide, isolated from *Staphylococcus aureus* in the form of a powder and dissolved at a 7 concentration of 1 mg/mL in ultrapure water. For use, samples were diluted to the designated concentration using a buffer solution and stored at 4 ℃. We previously reported a *de novo* designed β-hairpin peptide (SVG28) that assembles to form a β-barrel nanopore structure in the BLMs. SVG28 was dissolved at a concentration of 100 μM in ultrapure water: DMSO = 1:1 (v/v) and stored at -30 °C. The solid phase synthesis of SVG28 and the confirmation of synthesis is described in our previous paper.[7]

Properties of four different block copolymers

The properties of PBD11, PBD22, PDMS22, and PDMS35 are summarized in **Table 1**. PBD11 and PBD22 share the same monomer composition but differ in molecular weight. Similarly, PDMS22 and PDMS35 differ in di- and tri-block configuration despite having a similar chemical structure. The hydrophilic volume fractions (*f*-ratios) and the polydispersity index (PDI) are listed in **Table 1**. PBDs are composed of more than 85% 1,2-butadiene, and PDMS22 is linked by benzyl chloride between PMOXA and PDMS.

Table 1 Lipid and polymer properties

Molecule	Abbreviation	Structure	Molecular weight [g/mol]	*f*-ratio	PDI	
DPhPC	DPhPC	Lipid	846.25	-	-	-
PBD11-b-PEO8	PBD11	Diblock polymer	950 (600-b-350)	0.37	1.06	1,2 addition Butadiene > 85%
PBD22-b-PEO14	PBD22	Diblock polymer	1800 (1200-b-600)	0.33	1.01	1,2 addition Butadiene > 85%
PDMS22-b-PMOXA6	PDMS22	Diblock polymer	2100 (1600-b-500)	0.24	1.12	Benzyl Chloride linker
PMOXA11-b-PDMS35-b-PMOXA11	PDMS35	Triblock polymer	4500 (950-b-2600-b-950)	0.42	1.3	-

Interfacial tension measurement

The interfacial tension at an oil-water interface coated with a lipid or polymer monolayer was evaluated by the pendant drop method (DMs-401, Kyowa Interface Science Co., Ltd). Measurements were made by generating either DPhPC or a polymer solution droplet at the tip of a J-shaped stainless steel reversed needle immersed in a cuvette containing a buffer solution. Each experiment was performed with the amount of droplets that stabilized the interfacial tension values. Prior to submersion, the needle was pre-loaded with the solution and thoroughly cleaned with water and ethanol both before and after each measurement. The interfacial tension values were calculated by the Young-Laplace method using the following density values for each solute: 1.04 g/cm^3 for 1 M KCl, 0.73 g/cm^3 for decane, and 1.49 g/cm^3 for chloroform. The density of the mixture of chloroform and decane was calculated from the volume ratio. The recorded data was analyzed using Excel (Microsoft, USA) software. The experiment was performed at a room temperature of 22 ± 2 °C. The number of experiments was repeated at least five times, and means and standard errors were calculated from the data obtained.

Contact angle measurement

To prepare water-in-oil (W/O) droplets coated with lipid or polymer monolayers, approximately 10 vol% buffer solution was added to either the DPhPC solution or the polymer solution. Emulsification was achieved by pipetting. After pipetting, the aliquot containing the droplet was placed between two cover glasses with spacers (Matsunami Glass Industries, Osaka, Japan). The aliquots were filled and sealed in the cover glass to

prevent the volatilization of chloroform in the polymer solution during observation.

The contact angle θ was determined from images of the W/O droplet pair taken along the equatorial plane using a fluorescence microscope (Olympus IX73, Olympus Corporation, Tokyo, Japan) with a 40× objective lens. W/O droplet pairs of similar sizes were used to analyze θ, where the droplet interface was observed in the focal plane and the oil-water interface coated with lipids or polymers can be seen as the black lines (**Fig. S5**). The pictures were analyzed using ImageJ software (Molecular Devices, San Jose, CA, USA) and Excel software (Microsoft, USA). The experiment was performed at a room temperature of 22 ± 2 °C. The number of experiments was repeated at least three times, and means and standard errors were calculated.

Preparation of microdevices

The microdevice was fabricated by machining a 6.0 mm thick, 10 × 10 mm polymethyl methacrylate (PMMA) plate (Mitsubishi Rayon, Tokyo, Japan) using a computer-aided design and computer-aided manufacturing three-dimensional modeling machine (MM-100, Modia Systems, Japan). Two wells (2.0 mm diameter and 4.5 mm depth) and a chase between the wells were manufactured on the PMMA plate. Each well had a through-hole in the bottom, and Ag/AgCl electrodes were set into this hole. A polymeric film made of polychloro-*p*-xylylene (parylene C) with a thickness of 5 μm was patterned with single pores (100 μm diameter) by the conventional photolithography method and then fixed between PMMA films (0.2 mm thick) using an adhesive bond (Super X, Cemedine Co., Ltd, Tokyo, Japan). The films, including the parylene C film, were inserted into the chase to separate the wells (**Fig. S1**).

Preparation of BLMs and BPMs

BLMs and BPMs were prepared using the microdevice as described in the following procedures: the wells of the micro device were filled with either DPhPC solution or polymer solution (0.8 μL). The buffer solution (4.7 μL) was poured into one chamber, which was connected to the ground terminal. The buffer solution (4.7 μL) was also poured into another chamber, which was connected to the recoding terminal. Within a few minutes of adding the solutions, BLMs and BPMs formed on a parylene C film that separated the two chambers. When membranes ruptured during this process, they were

reassembled by tracing with a hydrophobic stick at the droplet interface.

Membrane capacitance measurement

The membrane capacitance experiment was conducted by applying rectangular pulse voltage using an Axopatch 200B amplifier (Molecular Devices, San Jose, CA, USA). The rectangular pulse voltage was applied to the recording chamber, and the other was grounded in a constant voltage of 0 mV. The signals were detected using a 10 kHz low-pass Bessel filter at a sampling frequency of 50 kHz. The recorded data were analyzed using the Clampex 9.0 software (Molecular Devices, San Jose, CA, USA) and Excel software (Microsoft, USA). The experiment was performed at a room temperature of 22 ± 2 °C. The number of experiments was repeated at least six times, and means and standard errors were calculated.

Membrane stability measurement

The membrane lifetime experiment was conducted at a constant voltage of 0 mV using a JET patch clamp amplifier (Tecella, USA) and a Pocket patch clamp amplifier (Tecella, USA). The signals were detected using a 3.2 kHz low-pass Bessel filter at a sampling frequency of 20 kHz. When the membranes ruptured, we observed a leakage current signal (**Fig. S8**). The experiment was performed at a room temperature of 22 ± 2 °C. The experiment was repeated at least eleven times, and means and standard errors were calculated.

The voltage application experiment was conducted using rectangular pulse voltages increased by 50 mV every 1 ms (interval: 0.4 ms, duration 0.6 ms) from 0 V to 2 V using a pico patch clamp amplifier (Tecella, USA). The signals were detected using an 8 kHz low-pass Bessel filter at a sampling frequency of 40 kHz. When the membranes ruptured, we observed a leakage current signal (**Fig. S9**). The experiment was performed at a room temperature of 22 ± 2 °C. The experiment was repeated at least nine times, and means and standard errors were calculated.

Analysis of a leak signal was performed using pCLAMP ver. 11.0.3 (Molecular Devices, USA), and Excel software (Microsoft, USA).

Channel current measurement

αHL was dissolved in buffer solution to the designated concentration. The buffer solution with αHL was poured into one chamber, which was connected to the ground terminal. The buffer solution was also poured into another chamber, which was connected to the recoding terminal.

SVG28 peptide was first placed in 1 M KOH for 5 minutes to transfer the isoacyl dipeptide to the native dipeptide of Val and Ser. Next, HCl was added to adjust the pH to 7. Then, 5 μM of transformation SVG28, buffer solution, and polymer solution were added. Following this, the mixture was vortexed for 30 seconds and incubated at 37°C for 24 hours. The solution containing the polymer, SVG28, and buffer was poured into one chamber, which was connected to the ground terminal. The buffer solution was also poured into another chamber, which was connected to the recoding terminal.

The channel current was observed using JET patch clamp amplifier (Tecella, USA) and Pocket patch clamp amplifier (Tecella, USA). A constant voltage of +100 mV was applied to the recording chamber, and the other side was grounded. The pore-forming signals were detected using a 3.2 kHz low-pass Bessel filter at a sampling frequency of 20 kHz. Channel current signals were analyzed using pCLAMP ver. 11.0.3 (Molecular Devices, USA), and Excel software (Microsoft, USA). The experiment was performed at a room temperature of 22 ± 2 °C. The number of experiments was repeated at least three times, and means and standard errors were calculated.

Results and Discussion

Optimization of polymer solutions

For the preparation of BPMs by DCM, we typically use decane or *n*-hexadecane (hexadecane) for the oil phase, as previously reported,[18,19,21,22] but all polymers did not dissolve in them. Therefore, we investigated organic solvents that would allow the polymers to dissolve and mix with decane. Through solubility testing with ethanol, chloroform, and DMSO, we found that chloroform dissolves all copolymers and mixes with decane. Next, the ratio of chloroform-decane solvent was tested. The results demonstrated that PBD11 and PBD22 were capable of dissolution in a chloroform-decane solution at any ratio. Conversely, PDMS22 and PDMS35 exhibited incomplete dissolution at all ratios, accompanied by the formation of white precipitation within the chloroform-decane solvent system. Consequently, the solution comprising a 3:7 ratio of chloroform-decane was selected, and its supernatant was used in subsequent experiments.

The interfacial tension and adhesive energy of bilayer polymer membranes

Table 2 Membrane properties evaluated by interfacial tension and contact angles*

Membrane	Oil type	Monolayer tension [mN/m]	Contact angle [°]	Bilayer tension [mN/m]	Adhesive energy [mJ/m^2]	$\Delta F/2\gamma_m$ [% reduction]
DPhPC	decane	7.4 ± 1.0 *n*=10	19 ± 0.51 *n*=28	14 ± 1.9	0.79 ± 0.25	5.3
PBD11	3chloroform-7decane	2.8 ± 0.28 *n*=12	23 ± 0.91 *n*=30	5.2 ± 0.52	0.44 ± 0.061	7.8
PBD22	3chloroform-7decane	2.3 ± 0.12 *n*=5	21 ± 0.77 *n*=47	4.3 ± 0.22	0.32 ± 0.030	6.9
PDMS22	3chloroform-7decane	2.9 ± 0.16 *n*=10	18 ± 0.30 *n*=23	5.5 ± 0.31	0.27 ± 0.018	4.7
PDMS35	3chloroform-7decane	1.6 ± 0.088 *n*=10	20 ± 0.72 *n*=19	3.0 ± 0.17	0.18 ± 0.017	5.8

* Average values and standard errors were calculated.

To investigate the self-assembly of four types of amphiphilic polymers and to make a comparison with the conventional phospholipid (DPhPC) at the oil/aqueous interface, we first estimated the interfacial tension by the pendant drop method. We prepared DPhPC solution and polymer solution. **Fig. 2a** shows the changes in interfacial tension (γ) over time for inverted droplets of DPhPC solution in a buffer solution. The γ of DPhPC solution decreases from ~30 mN/m to an equilibrium value of 7.4 ± 1.0 mN/m

(**Table 1**) within ~2000 seconds. This value was consistent with the value at the interface of water/DPhPC dissolved in hexadecane in the previous reports with a lipid-out method,[22] and detailed results were described in **SI text** and **Fig. S2**.

Fig. 2b and **Fig. S4** show the changes in γ as a function of time for the polymer solution. The γ for each polymer changed to decrease to ~5 mN/m quickly during the first few seconds, after which the γ decreased more gradually over another ~1800 seconds. The value reached at 2.8 mN/m for PBD11, 2.3 mN/m for PBD22, 2.9 mN/m for PDMS22, and 1.6 mN/m for PDMS35 in 1800 seconds measurement. The time for all polymers to reach the equilibrium state was faster than that of DPhPC, suggesting that the polymers may form a monolayer at the interface more rapidly than DPhPC. Comparing PBD11 and PBD22, PBD22 had a γ value 1.2 times lower than that of PBD11 (2.8 and 2.3 mN/m). In contrast, in the case of PDMS22 and PDMS35, PDMS35 showed a γ value 1.8 times lower than that of PDMS22 (2.9 and 1.6 mN/m). The lower interfacial tension in PDMS35 could be attributed to its tri-block configuration. Specifically, the tri-block structure may allow for tighter packing, leading to a reduced amount of residual oil, and the tri-block configuration may result in decreased polymer-polymer interactions compared to the di-block configuration of PDMS22.

To calculate the bilayer tension and adhesive energy of BPMs, we measured the contact angles (θ) of polymer W/O droplets.[23] **Fig. 2c-g** and **Fig. S6** show the histograms of the contact angle between the adhering droplets of the buffer solution in DPhPC or polymer solutions. The average values of the contact angles after 2 hours of preparation are shown in **Fig. 2c-g** and summarized in Table 2. The θ values for PBD11 and PDMS35 were slightly higher, while those for DPhPC, PBD22, and PDMS22 remained nearly identical. The average θ value of DPhPC was comparable to 15.4° in previous research.[24] The bilayer tension (γ_b) was calculated from the average θ values. When assembling bilayer membranes using DCM, the γ_b is balanced by the two-monolayers tension (γ_m) at the annulus bulk phase-water interface oriented away from the plane of the membrane by the contact angle θ, via Young's relationship[15,24,25] (**Fig. S1c**):

$$\gamma_b = 2\,\gamma_m \cos\theta$$

The values of γ_b for DPhPC in lipid-out method were 14 mN/m, whereas previous research reported the DPhPC of γ_b values in lipid-in method were 2.1 mN/m.[24] These differences were derived from a higher estimation of γ_m in this study, and further discussions were described in **SI text** and **Fig. S2**. **Table. 2** shows that the γ_b values were 5.2 mN/m for PBD11, 4.3 mN/m for PBD22, 5.5 mN/m for PDMS22, and 3.0 mN/m for PDMS35. The different γ_b values of each BPM may affect the interaction of nanopores.

Finally, the adhesive energy, *ΔF*, was calculated using[15,25]:

$$\Delta F = 2\,\gamma_m - \gamma_b$$

The adhesive energy reflects the reduction in the system's free energy gained by replacing the opposing monolayer-coated regions of the droplets with a shared bilayer interface. Alternatively, it can be interpreted as the energy per unit area required to separate the attached droplets. The *ΔF* depends on the choice of surfactant and oil.[15] The values of *ΔF* showed that from 0.18 to 0.79 mJ/m^2 (**Table 2**). The values of *ΔF* were in the order: DPhPC > PBD11 > PBD22 > PDMS22 > PDMS35. The ratio of the free energy of the bilayer and two monolayer membranes ($\gamma_b/2\gamma_m$) was determined by dividing the adhesive energy by the monolayer tension of two droplets (*ΔF*/$2\gamma_m$).[15] The values of *ΔF*/ $2\gamma_m$ were also listed in **Table 2**, and the order is: PBD11 > PBD22 > PDMS35 ~ DPhPC > PDMS22. In the case of DPhPC, the value of *ΔF* was high, but *ΔF*/$2\gamma_m$ was medium compared to BPMs due to the higher estimation of γ_m of DPhPC. Both the value of *ΔF* and *ΔF*/$2\gamma_m$ of PBD11 was high, which may affect the stability of membranes, as we discussed in the following section.

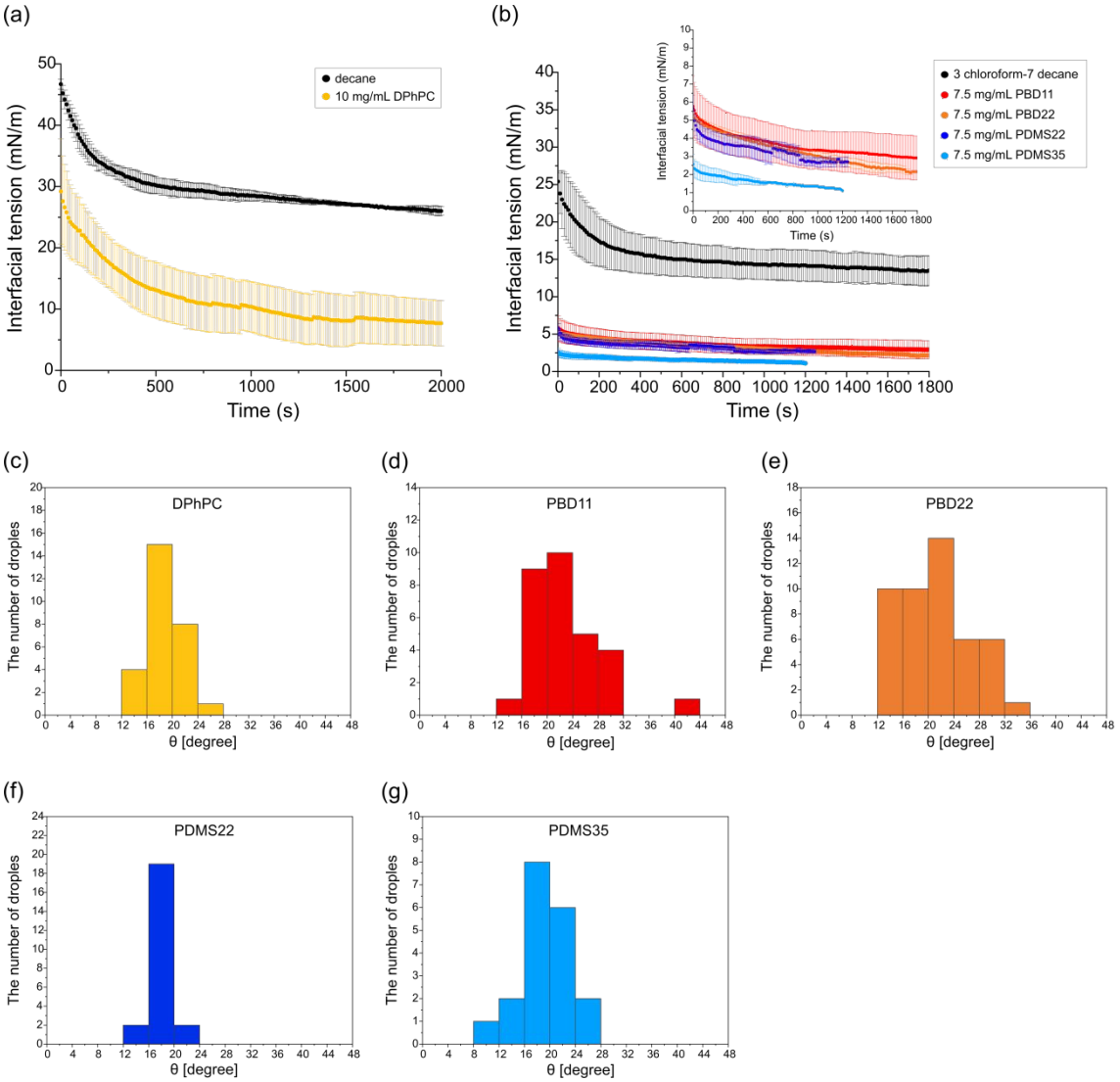

Fig. 2 (a, b) Interfacial tension versus time measured at (a) DPhPC solution/buffer solution, and (b) polymer solution/buffer solution. (c-g) The histogram of contact angle between adhering DPhPC or polymer W/O droplets after 2 hours. The membrane molecule types are (c) DPhPC, (d) PBD11, (e) PBD22 (f) PDMS22, and (g) PDMS35.

Electrical characterization of bilayer polymer membranes

Table. 3 Membrane properties evaluated by electrophysiology*

Membrane	Membrane Capacitance [pF]	Hydrophobic thickness [nm]	Lifetime [s]	Rupture voltage [mV]	Rupture electric field [mV/nm]	Pore signal appearance [s^{-1}]	RMS noise [pA]	Pore conductance [nS]
DPhPC	17.8 ± 1.83 *n*=20	3.3 ± 0.33	2998 ± 904 n=11	467 ± 38 *n*=15	141 ± 23	0.32 ± 0.104 *n*=11	1.51 ± 0.20 *n*=19	1.11 ± 0.035 *n*=19
PBD11	12.9 ± 0.61 *n*=20	4.4 ± 0.23	2741 ± 632 *n*=14	917 ± 65 *n*=30	208 ± 19	0.021 ± 0.007 *n*=8	1.77 ± 0.10 n=39	0.70 ± 0.020 n=44
PBD22	7.65 ± 0.48 *n*=18	7.7 ± 0.51	3390 ± 586 n=17	1226 ± 48 *n*=36	159 ± 13	0 *n*>10	n/a	n/a
PDMS22	11.5 ± 0.33 *n*=6	5.3 ± 0.16	60 ± 18.5 *n*=42	583 ± 89 *n*=9	110 ± 17	0 *n*>10	n/a	n/a
PDMS35	11.8 ± 0.59 *n*=8	5.3 ± 0.27	205 ± 71.9 n=20	667 ± 44 *n*=9	126 ± 11	0.129 ± 0.037 *n*=4	4.31 ± 0.89 *n*=7	1.26 ± 0.098 *n*=14

* Average values and standard errors were calculated.

Next, we attempted to prepare polymer bilayers with DCM in the microdevices. The BPMs made from four amphiphilic polymers were formed in this system. The membrane capacitance was measured to evaluate the membrane's hydrophobic thickness. The value of membrane capacitance is related to the membrane's hydrophobic thickness, membrane area, and dielectric constant by the following equation[15,24–26].

$$Cm = \varepsilon_0 \varepsilon \frac{S}{d}$$

where C_m represents the membrane capacitance, S is the membrane area, ε_0 is the dielectric permittivity of vacuum (8.85×10^{12} Fm^{-1}), ε is the relative permittivity of the hydrophobic region of the membrane, and d is the hydrophobic thickness of the membrane. The adhesion of two droplets, each coated with amphiphilic molecules, to each other, due to the combined action of van der Waals forces and hydrodynamic pressure, results in an increase in the contact area (S) and a concomitant decrease in the hydrophobic thickness (d). This change leads to an increase in membrane capacitance (C_m). Once the opposing monolayers come close enough for short-range repulsive forces to dominate, the increase in C_m stabilizes, and these forces help prevent droplet coalescence.[15] It was observed that the membrane capacitance of four BPMs increased and then reached a stable value of 0 mV, which was also seen in the DPhPC (**Fig. S7a**).

The average C_m values are summarized in **Table 3** and **Fig. 3a**. From the membrane capacitance values, we next calculated the membrane's hydrophobic thickness. We used ε as 2.2 for DPhPC,[24,26] 2.5 for PBD11 and PBD22,[25] and 2.8 for PDMS22 and PDMS35[15] from literature. For the membrane area, we assumed an average diameter of 56 μm in the diameter of 100 μm diameter pore in supported film (parylene C film) based on previous research.[27] Under this assumption, the calculated hydrophobic thickness is 3.3 nm for DPhPC, 4.4 nm for PBD11, 7.7 nm for PBD22, 5.3 nm for PDMS22, 5.3 nm for PDMS35, as presented in **Fig. 3b**. The result of 3.3 nm for DPhPC was comparable to 4 nm for DPhPC prepared by DCM reported in previous research by G.J. Taylor *et al.,*[24] supporting our assumption.

The polymer chain structures in BPMs are considered. It is observed that the hydrophobic tails adopt coiled conformations, with segments undergoing a random walk under conditions of low polymer concentration. The hydrophobic thickness h is given by[28]:

$$h = 2 \times Rf$$

where Rf is the Flory radius of the polymer. The flory radius is described by the equation[29]:

$$Rf = N^{3/5} \times a$$

where Rf represents the Flory radius, N is the number of hydrophobic polymer segments, and a is the segment length. PBD11 and PBD22 consist of approximately 11 and 22 repeat units of 1,2-butadiene, respectively. PDMS22 and PDMS35 consist of approximately 22 repeat units and 35 repeat units of PDMS, respectively. The segment length a is reported to be 0.6 nm for both PDMS[15,30] and 1,2-butadiene[31] in the literature. Based on this segment length, the Rf is estimated to be 2.5 nm for PBD11, 3.8 nm for PBD22, 3.8 nm for PDMS22, and 5.1 nm for PDMS35. Thus, the predicted hydrophobic thicknesses are approximately 5.0 nm for PBD11, 7.6 nm for PBD22, 7.6 nm for PDMS22, and 10.2 nm for PDMS35. Comparing these calculated values with those obtained from membrane capacitance measurements, the predicted thicknesses for PBD11 (5.0 nm) and PBD22

(7.6 nm) are in good agreement with the measured value of PBD11 (4.4 nm) and PBD22 (7.7 nm). On the other hand, the predicted thicknesses of PDMS22 (7.6 nm) and PDMS35 (10.2 nm) are higher than the measured values of PDMS22 (5.3 nm) and PDMS35 (5.3 nm). This difference may be due to the laterally swollen conformation of the PDMS series in the chloroform-decane solvent system.

To measure the lifetime of BPMs, we next measured the lifetime of the membrane (t_m) under 0 V for 150 mins. The t_m was defined from 0 sec (after the C_m value of was stable) to the time of the membrane rupture or time of 150 mins. The t_m of BPMs was assessed by the survival rate.

$$\text{Survival rate [\%]} = 1 - \frac{\text{the number of the membrane ruptures at time } a}{\text{the number of DCM experiments}}$$

where time a is the time to rupture the membrane, defined as time 0 when the capacitance value of the membrane has stabilized. **Fig. 3c** shows the survival rate of DPhPC and four polymers. The average value of t_m was 2998 seconds for DPhPC, 2741 seconds for PBD11, 3390 seconds for PBD22, 60 seconds for PDMS22, and 205 seconds for PDMS35. The t_m of PBD11 and PBD22 were similar or slightly longer than DPhPC; on the contrary, PDMS22 and PDMS35 were observed to rupture within a few minutes and did not maintain an insulator by 30 min in all experiments.

We next applied stepping pulse-voltages increasing by 50 mV every 1 ms (0, 50, 100, 150 mV….), with a pulse duration of 0.6 ms and an interval of 0.4 ms, and observed the membrane rupture.[15,32] The average rupture voltages (V_m) were 467 mV for DPhPC, 917 mV for PBD11, 1226 mV for PBD22, 583 mV for PDMS22, and 667 mV for PDMS35 (**Fig. 3d**). As the hydrophobic thickness, d, increased, the value of V_m was higher (**Fig. S10a**). This trend is consistent with previous research, where BPMs are more resistant to electroporation with increased thickness.[15] The E_m[15] value, which is determined by dividing the rupture voltage by the hydrophobic thickness, are calculated as 141 mV/nm for DPhPC, 208 mV/nm for PBD11, 159 mV/nm for PBD22, 110 mV/nm for PDMS22, 126 mV/nm for PDMS35. Compared to PBD11 and PBD22, the E_m value of PBD11 was 1.3 times higher than that of PBD22, whereas the PDMS series were similar.

Next, we consider the relationship between membrane properties ($\Delta F/2\gamma_m$, t_m, and E_m). **Fig. 3e** and **Fig. S10b-c** present a scatter plot illustrating the interrelationships among these parameters. The correlation coefficient was 0.88 between $\Delta F/2\gamma_m$ and E_m, suggesting that the value of $\Delta F/2\gamma_m$ has a potential value for predicting the membrane stability.

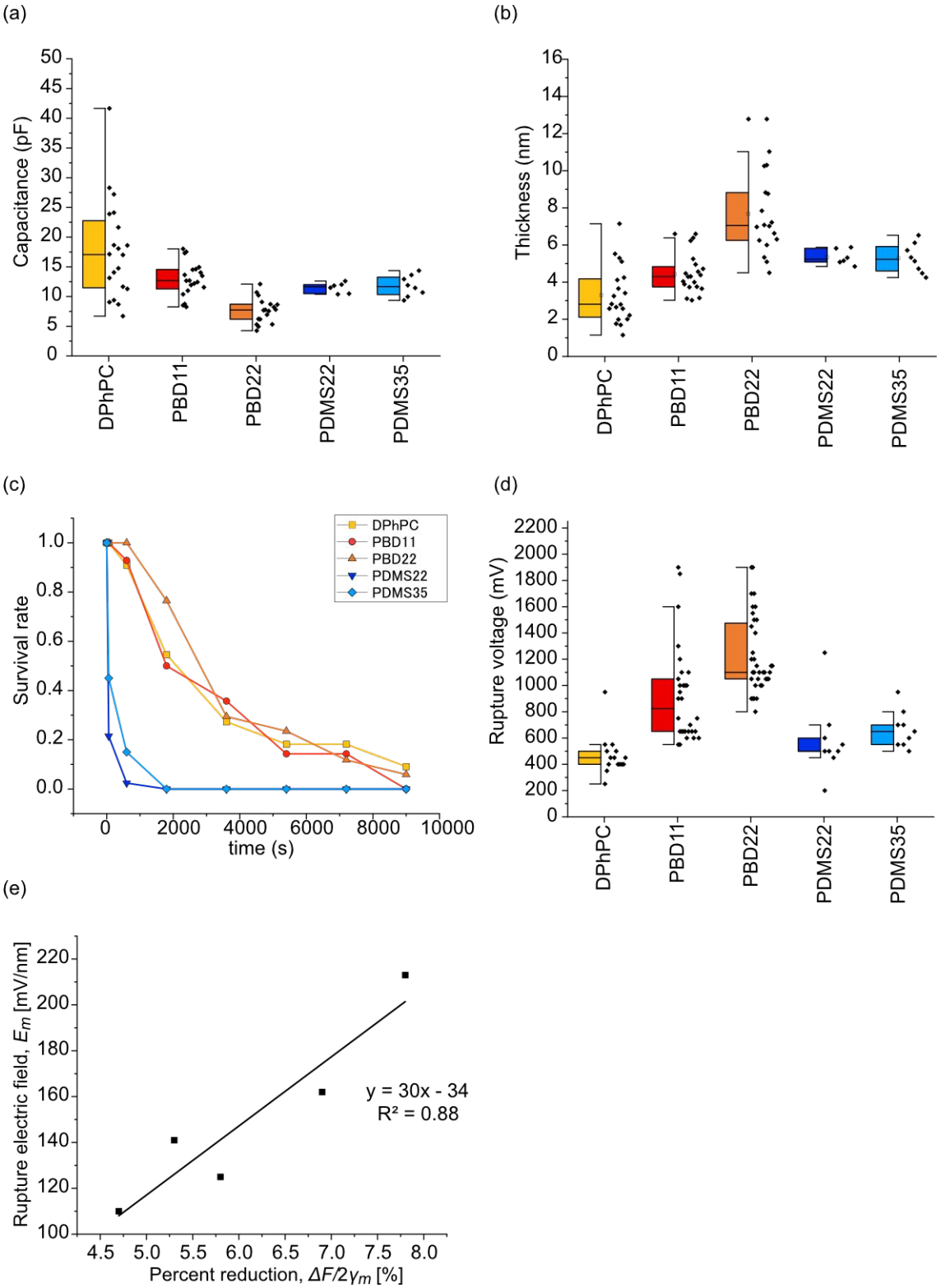

Fig. 3 (a) The boxplot of the membrane capacitance of BLMs and BPMs at 0 mV. (b) The boxplot of the hydrophobic thickness of BLMs and BPMs determined from membrane capacitance in (a). (c) The survival rate at BLMs and BPMs at 0 mV. (d) The

boxplot of the rupture voltage of BLMs and BPMs. (e) The scatter plot of the relationship between rupture electric field, E_m, and percent reduction of free energy, $\Delta F/2\gamma_m$.

Nanopore reconstitution in BPMs

To investigate the effect of BPMs composition on the reconstitution of nanopores, we conducted channel current measurements of αHL nanopores with four different BPMs at 100 mV. The results showed successful reconstitution of αHL nanopores into PBD11 and PDMS35, but no reconstitution into PBD22 and PDMS22 (**Fig. 1**). This may be due to the membrane thickness inconsistency: the αHL nanopore's transmembrane length is 5.2 nm[33] while the hydrophobic thickness of BPMs was 4.4 nm for PBD11, 7.7 nm for PBD22, 5.3 nm for PDMS22 and 5.3 nm for PDMS35. As shown in Table 3, PDMS22 exhibits a membrane lifetime of approximately 60 seconds, and membrane rupture was observed within a similar or shorter timeframe during the nanopore reconstitution experiments. Within this limited timeframe, we believe we will not be able to confirm the formation of αHL pores.

To evaluate the probability of pore formation of BPMs, the pore signal appearance frequency of 1 μM αHL nanopores in DPhPC, PBD11, and PDMS35 membranes was measured. The pore signal appearance frequencies were 0.32 s^{-1} for DPhPC, 0.021 s^{-1} for PBD11 and 0.13 s^{-1} for PDMS35 (**Fig. 4a**). The stronger polymer interaction of PBD11 causes stronger molecular packing, and it may hinder pore-formation. On the other hand, PDMS35 is believed to have flexibility and fluidity similar to that of phospholipid bilayers, probably due to its molecular configuration.[17] The values of E_m and γ_b of PBD11 and PDMS35 suggest that PDMS35 has weaker intermolecular interactions than PBD11, which is thought to facilitate the reconstitution of αHL nanopores.

To further assess the intermolecular interaction between the αHL nanopore and BPMs, we calculated the root-mean-square (RMS) noise of the open pore state.[34] The results showed 1.5 pA for DPhPC, 1.8 pA for PBD11, and 4.3 pA for PDMS35 (**Fig. 4b**). The RMS noise in the PDMS35 was relatively large because of the appearance of the gating-like noise (**Fig. S12**). D. Morton *et al.* reported that the gating-like noise has also been observed in MspA nanopores within PMOXA-PDMS-PMOXA membranes, and this noise may be due to both the balance of the hydrophilic-hydrophobic ratio (*f*-ratio)

and the hydrophobic mismatch between the transmembrane pore and membranes.[11] Although the hydrophobic thickness of PDMS35 was close to the transmembrane length of αHL (5.2 nm for αHL and 5.3 nm for PDMS35), the *f*-ratio was different between BPMs as 0.42 for PDMS35 and 0.37 for PBD11(**Table 1**). Another possible reason was the difference of γ_b. The higher bilayer tension may keep the nanopores from fluctuating in the membrane (5.2 mN/m for PBD11 and 3.0 mN/m for PDMS35).

The conductance of αHL nanopores embedded in DPhPC, PBD11, and PDMS35 was measured. The result showed the peak conductance of 1.11 nS for DPhPC, 0.70 nS for PBD11, and 1.26 nS for PDMS35 (**Fig. 4c-e**). DPhPC and PDMS35 had similar peak conductance values; conversely, the conductance of PBD11 was approximately 36% lower than that of DPhPC. To consider the difference between the low and high conductance, we compared measured conductance values with those predicted from Hill's equation given by:

$$G = \frac{V}{I} = \sigma\left(\frac{4l}{\pi d^2} + \frac{1}{p}\right)^{-1}$$

where G is pore conductance, I is current through the pore, V is the applied voltage between two chambers, l is the pore length, σ is ionic conductivity (10.5 S/m for 1M KCl[35]), and p is the pore diameter. Based on Hill's equation, the decrease of conductance is due to the increase in pore length, l, and the decrease in pore diameter, p. (**Fig. S13**). In the case of PBD11, there are highly dense PEO chains in the vicinity of the pore. The decrease in conductance may be caused by an increase in effective pore length due to the PEO chains, and detailed discussions are described in **SI text** and **Fig. S13**.

We investigated the effect of BPMs' composition on the reconstitution of αHL nanopores and revealed that PBD11 has membrane properties of pore-forming ability and low electrical noise for αHL. From this result, we anticipated that PBD11 could demonstrate these membrane properties not only for αHL but also for wider range of other nanopores, particularly *de novo* designed peptide nanopores with β-barrel structure, SVG28.[7] The SVG28 nanopore was reconstituted into PBD11 (**Fig. 4f**). SVG28 was designed to form nanopores with a transmembrane length close to the thickness of the

lipid membrane, which may also be near the hydrophobic thickness of PBD11. Detailed results were described in **SI text** and **Fig. S14**.

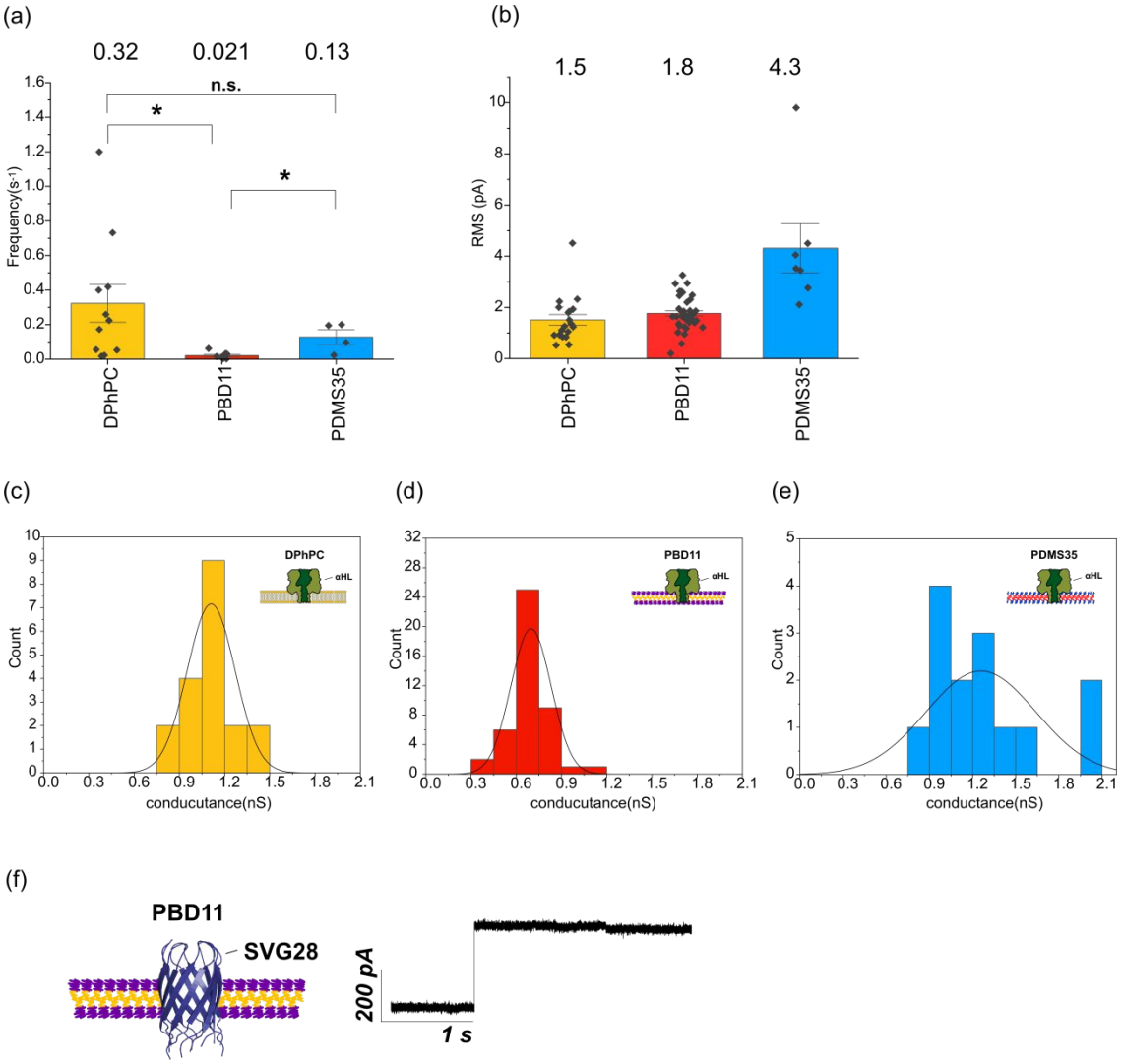

Fig. 4 (a-e) Analysis of signals obtained from αHL nanopores at 100 mV. (a) Comparison of the pore signal appearance frequency of 1 μM αHL of DPhPC, PBD11, and PDMS35. * denotes significant differences, where $p < 0.05$ and error bars represent standard errors. (b) Comparison of the RMS noise of αHL of DPhPC, PBD11, and PDMS35. (c-e) Histogram of open conductance formed by αHL nanopores in (c) DPhPC, (d) PBD11, and (e) PDMS35. (f) Pore-forming signals from SVG28 nanopores embedded in PBD11 at 100 mV.

Conclusions

We investigated the membrane properties of various BPMs made from four different polymers and their effects on nanopore reconstitution. The polymers (PBD11, PBD22, PDMS22, and PDMS35) were studied for their ability to self-assemble at the oil/aqueous interface, showing faster monolayer formation than DPhPC. Using monolayer tension and contact angle, we estimated the bilayer tension and adhesive energy ratio ($\Delta F/2\gamma_m$) of these BPMs. We also prepared four types of BPMs using a microdevice and measured their hydrophobic thickness and stability. Our results showed that the PBD series had higher stability over time and voltage than the PDMS series. Importantly, correlation analysis identified a strong relationship between $\Delta F/2\gamma_m$ and membrane stability, indicating $\Delta F/2\gamma_m$ as a promising predictive parameter for membrane properties. For αHL nanopores, channel currents were reconstructed with PBD11 and PDMS35 but not with PBD22 and PDMS22, likely due to mismatches between nanopore length and BPM hydrophobic thickness. Ion current measurements revealed that PDMS35 had a higher signal frequency, while PBD11 produced less electrical noise. PBD11 also worked with the artificial nanopore SVG28. To advance nanopore sensing applications, optimizing BPM properties for specific nanopores (e.g., αHL, MspA, CsgG, aerolysin, and artificial designs) is crucial. This study offers a foundation for understanding which BPMs are more stable and suitable for nanopores. Further research using high-throughput systems like DCM could provide deeper insights into various BPM-nanopore combinations. These findings will not only contribute to nanopore technologies, including nanopore protein sequencing[36] or microRNA diagnostics[37] but also to future technologies in engineering biology[38] or molecular robotics[39].

Author contributions

R.K. conceived the original idea. H.K. performed all experiments. M.S. conducted experiments related to the preparation of BPMs and channel current measurements. H.K. and R.K. wrote the manuscript, and R.K. supervised the entire research. All authors approved the final version of the manuscript.

Data availability

The data supporting this article has been included as part of the ESI.

Conflicts of interest

There are no conflicts to declare.

Acknowledgments

This research was partially supported by JSPS KAKENHI, grant numbers 21K19786 and 21H05229, and JST-CREST JPMJCR21B2. The authors would like to acknowledge the use of DeepL Write and Grammarly for the purposes of language editing.

Reference

1 S. M. Bezrukov, I. Vodyanoy and V. A. Parsegian, *Nature 1994 370:6487*, 1994, **370**, 279–281.
2 Y. L. Ying, Z. L. Hu, S. Zhang, Y. Qing, A. Fragasso, G. Maglia, A. Meller, H. Bayley, C. Dekker and Y. T. Long, *Nature Nanotechnology 2022 17:11*, 2022, **17**, 1136–1146.
3 J. J. Kasianowicz, E. Brandin, D. Branton and D. W. Deamer, *Proc Natl Acad Sci U S A*, 1996, **93**, 13770–13773.
4 M. Jain, H. E. Olsen, B. Paten and M. Akeson, *Genome Biology 2016 17:1*, 2016, **17**, 1–11.
5 H. Watanabe, A. Gubbiotti, M. Chinappi, N. Takai, K. Tanaka, K. Tsumoto and R. Kawano, *Anal Chem*, 2017, **89**, 11269–11277.
6 J. R. Burns, A. Seifert, N. Fertig and S. Howorka, *Nat Nanotechnol*, 2016, **11**, 152–156.
7 K. Shimizu, B. Mijiddorj, M. Usami, I. Mizoguchi, S. Yoshida, S. Akayama, Y. Hamada, A. Ohyama, K. Usui, I. Kawamura and R. Kawano, *Nat Nanotechnol*, 2022, **17**, 67–75.
8 M. Langecker, V. Arnaut, T. G. Martin, J. List, S. Renner, M. Mayer, H. Dietz and F. C. Simmel, *Science (1979)*, 2012, **338**, 932–936.
9 A. A. Vorobieva, P. White, B. Liang, J. E. Horne, A. K. Bera, C. M. Chow, S. Gerben, S. Marx, A. Kang, A. Q. Stiving, S. R. Harvey, D. C. Marx, G. Nasir Khan, K. G. Fleming, V. H. Wysocki, D. J. Brockwell, L. K. Tamm, S. E. Radford and D. Baker, *Science (1979)*, DOI:10.1126/SCIENCE.ABC8182/ASSET/BB42ADB1-F105-4177-AEB1-4B71D7F50484/ASSETS/GRAPHIC/371_ABC8182_F6.JPEG.
10 A. González-Pérez, K. B. Stibius, T. Vissing, C. H. Nielsen and O. G. Mouritsen, *Langmuir*, 2009, **25**, 10447–10450.
11 D. Morton, S. Mortezaei, S. Yemenicioglu, M. J. Isaacman, I. C. Nova, J. H. Gundlach and L. Theogarajan, *J Mater Chem B*, 2015, **3**, 5080–5086.
12 L. Yu, X. Kang, M. A. Alibakhshi, M. Pavlenok, M. Niederweis and M. Wanunu, *Biophys J*, 2021, **120**, 1537–1541.
13 C. Nardin, M. Winterhalter and W. Meier, *Langmuir*, 2000, **16**, 7708–7712.
14 W. Meier, C. Nardin and M. Winterhalter, *Angewandte Chemie - International Edition*, 2000, **39**, 4599–4602.
15 N. Tamaddoni, G. Taylor, T. Hepburn, S. Michael Kilbey and S. A. Sarles, *Soft Matter*, 2016, **12**, 5096–5109.
16 D. Wong, T. J. Jeon and J. Schmidt, *Nanotechnology*, 2006, **17**, 3710–3717.
17 S. Groeer, M. Garni, A. Samanta and A. Walther, *ChemSystemsChem*, 2022, **4**, e202200009.
18 R. Kawano, Y. Tsuji, K. Sato, T. Osaki, K. Kamiya, M. Hirano, T. Ide, N. Miki and S. Takeuchi, *Sci Rep*, 2013, **3**, 1–7.
19 R. Kawano, Y. Tsuji, K. Kamiya, T. Kodama and T. Osaki, *PLoS One*, 2014, **9**, 102427.
20 Y. L. Yang, M. Y. Chen, H. K. Tsao and Y. J. Sheng, *Physical Chemistry Chemical Physics*, 2018, **20**, 6582–6590.
21 K. Funakoshi, H. Suzuki and S. Takeuchi, *Anal Chem*, 2006, **78**, 8169–8174.
22 G. A. Venkatesan, J. Lee, A. B. Farimani, M. Heiranian, C. P. Collier, N. R. Aluru and S. A. Sarles, *Langmuir*, 2015, **31**, 12883–12893.
23 M. Yanagisawa, T. A. Yoshida, M. Furuta, S. Nakata and M. Tokita, *Soft Matter*, 2013, **9**, 5891–5897.
24 G. J. Taylor, G. A. Venkatesan, C. P. Collier and S. A. Sarles, *Soft Matter*, 2015, **11**, 7592–7605.
25 S. Koner, J. Tawfik, F. Mashali, K. B. Kennison, W. T. McClintic, F. A. Heberle, Y. M. Tu, M. Kumar and S. A. Sarles, *Biochimica et Biophysica Acta (BBA) - Biomembranes*, 2022, **1864**, 183997.
26 G. Cho, K. Kim, W. Chen, S. Son, T. J. Jeon and S. M. Kim, *Chemical Engineering Journal*, 2024, **495**, 153407.
27 H. Suzuki, K. V. Tabata, H. Noji and S. Takeuchi, *Langmuir*, 2006, **22**, 1937–1942.
28 G. J. Taylor, Y. Luo, K. Hong, S. A. Sarles, R. L. Sacci, B. Doughty and C. P. Collier, DOI:10.26434/CHEMRXIV.12106773.V2.

29 P. G. de Gennes, *Macromolecules*, 1980, **13**, 1069–1075.
30 G. Beaucage, S. Sukumaran, S. J. Clarson, M. S. Kent and D. W. Schaefer, *Macromolecules*, 1996, **29**, 8349–8356.
31 F. S. Bates, L. J. Fetters and G. D. Wignall, *Macromolecules*, 1988, **21**, 1086–1094.
32 M. Winterhalter, *Adv Colloid Interface Sci*, 2014, **208**, 121–128.
33 L. Song, M. R. Hobaugh, C. Shustak, S. Cheley, H. Bayley and J. E. Gouaux, *Science (1979)*, 1996, **274**, 1859–1866.
34 S. Fujita, I. Kawamura and R. Kawano, *ACS Nano*, 2023, **17**, 3358–3367.
35 W. Zhou, H. Qiu, Y. Guo and W. Guo, *Journal of Physical Chemistry B*, 2020, **124**, 1611–1618.
36 J. Ritmejeris, X. Chen and C. Dekker, *Nature Reviews Bioengineering 2024*, 2024, 1–14.
37 S. Takiguchi, N. Takeuchi, V. Shenshin, G. Gines, A. J. Genot, J. Nivala, Y. Rondelez and R. Kawano, *Chem Soc Rev*, DOI:10.1039/D3CS00396E.
38 M. B. Sheets, J. T. Atkinson, M. P. Styczynski and E. R. Aurand, *ACS Synth Biol*, 2023, **12**, 1574–1578.
39 Z. Peng, S. Iwabuchi, K. Izumi, S. Takiguchi, M. Yamaji, S. Fujita, H. Suzuki, F. Kambara, G. Fukasawa, A. Cooney, L. Di Michele, Y. Elani, T. Matsuura and R. Kawano, *Lab Chip*, 2024, **24**, 996–1029.

Data availability

All datasets underlying the findings of this study are provided in the Electronic Supplementary Information (ESI). In addition, detailed data used to generate the figures and other key findings can be obtained from the corresponding author upon a reasonable request.